Quantum Simulation of Solution Phase Intramolecular Electron Transfer Rates in Betaine-30

ARTICLE *in* THE JOURNAL OF PHYSICAL CHEMISTRY A · OCTOBER 2006

Impact Factor: 2.69 · DOI: 10.1021/jp063222d · Source: PubMed

3 AUTHORS, INCLUDING:

Hyonseok Hwang
Kangwon National University
29 PUBLICATIONS **401** CITATIONS

SEE PROFILE

ARTICLES

Quantum Simulation of Solution Phase Intramolecular Electron Transfer Rates in Betaine-30

Hyojoon Kim*,†

Chemical Physics Theory Group, Department of Chemistry, University of Toronto, Toronto, Ontario M5S 3H6, Canada

Hyonseok Hwang and Peter J. Rossky*,‡

Institute for Theoretical Chemistry, Department of Chemistry and Biochemistry, University of Texas, Austin, Texas 78712-1167

Received: May 25, 2006; In Final Form: August 7, 2006

Mixed quantum-classical atomistic simulations have been carried out to investigate the mechanistic details of excited state intramolecular electron transfer in a betaine-30 molecule in acetonitrile. The key electronic degrees of freedom of the solute molecule are treated quantum mechanically using the semiempirical Pariser−Parr−Pople Hamiltonian, including the solvent influence on electronic structure. The intramolecular vibrational modes are also treated explicitly at a quantum level, with the remaining elements treated classically using empirical potentials. The electron-transfer rate, corresponding to $S_1 \rightarrow S_0$ relaxation, is evaluated via time-dependent perturbation theory with the explicit inclusion of the dynamics of solvation and intramolecular conformation. The calculations reveal that, while solvation dynamics is critical to the rate, the intramolecular torsional dynamics also plays an important role. The importance of the use of multiple high-frequency quantum modes is also discussed.

I. Introduction

Since electron transfer (ET) processes are ubiquitous in a large variety of chemical and biological reactions, many recent theoretical and experimental studies have been devoted to understanding the details and mechanisms of ultrafast ET reactions.[1] In particular, intramolecular ET has been a primary focus in recent research because the contributions of diffusional encounter can be avoided, and the process can be photoinitiated. For such an ultrafast ET reaction, nonequilibrium solvation effects and the details of the accessible intramolecular vibrational energy levels have been inferred to play a crucial role. To incorporate these nonequilibrium effects on the ET rate, Sumi and Marcus described the dynamics with a formulation including a low-frequency classical vibrational degree of freedom in addition to a diffusional evolution of a classical solvation coordinate.[2] Jortner and Bixon pointed out that for electronic excited state ET, the potential impact of high-frequency vibrational modes was to introduce a manifold of vibrationally hot ground-state levels as potential ET product vibronic surfaces.[3] The treatment of both a diffusive solvent coordinate and a quantized intramolecular vibrational mode was incorporated into an accessible low-dimensional hybrid model by Barbara and co-workers[4] to account for their experimental results for intramolecular ET of a solvated betaine-30 dye molecule.

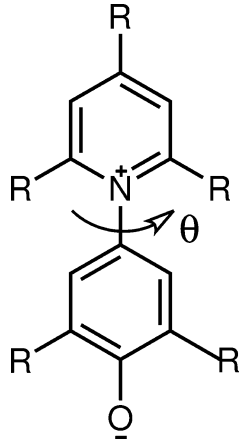

Figure 1. Molecular structure of a betaine dye. For betaine-30, the pendant group R = C_6H_5 and for the simplest betaine, R = H.

The structure of a betaine molecule (a substituted pyridinium *N*-phenolate) is shown in Figure 1, where for betaine-30, the pendant R groups are phenyl rings.

The betaine-30 dye molecule is one of the most sensitive solvatochromic probes and has been exploited as the basis for the E_T solvent polarity scale of more than 300 solvents.[5] Since the ET reaction can be controlled by solvation dynamics or vibrational Franck−Condon factors, or both, depending on the time scale for solvation dynamics, betaine-30 has been a target molecule to explore the kinetics of ET in a relatively compre-

† E-mail: hkim@chem.utoronto.ca. Telephone: (416)-978-6106. Fax: (416)-978-5325.
‡ E-mail: rossky@mail.utexas.edu. Telephone: (512) 471-3555. Fax: (512) 471-1624.

10.1021/jp063222d CCC: $33.50
Published on Web 09/12/2006

hensive series of experiments.[4,6−13] In addition, the most recent experiments on this system[13] have been interpreted as also reflecting intramolecular torsional dynamics, which was suggested as an important degree of freedom by earlier simulations from our lab.[14,15]

The hybrid model mentioned above generally successfully reproduced temperature and solvent dependences of experimental data, with a model consisting only of a classical diffusive solvent mode, with a single low-frequency and single high-frequency solute vibrational mode. However, it is of considerable interest to see to what extent such a model with a small number of empirically derived parameters accurately captures the high dimensional molecular system. Further, it has been suggested that the use of more realistic multiple time scale responses, including the fastest inertial time scale, is important for the proper description of the true ET dynamics.[16−18] Inertial solvent relaxation processes occur on the tens to hundreds of femtoseconds time scale, and slower diffusional solvent motions occur on the picosecond time scale.[19] Since the inertial solvent relaxation can account for a large fraction of the electronic energy gap dynamics, the relative importance of the two regimes will depend on the accessible final vibronic states of the reactant. Hence, there still exist important unclarified issues that could be answered from a detailed description of the experimentally studied system.

In earlier work from this lab,[14,15] practical mixed quantum-classical simulation methods for such large molecular systems were presented which treated most of the molecular elements in microscopic detail. The important quantum mechanical degrees of freedom, including electronic state, were treated explicitly, with a surface-hopping algorithm for nonadiabatic electronic transitions. These studies successfully reproduced a number of properties, such as the absorption intensity, width, and position of the S_0 to S_1 band. They also revealed interesting elements, including the fact noted above, that the transition energy is strongly coupled with the central dihedral ring angle (θ in Figure 1), that angle having the gas-phase S_1 excited-state minimum (and the minimum energy gap) for perpendicular rings. However, they were not able to evaluate a back ET $S_1 \rightarrow S_0$ rate, since that work used an unrealistic approximation for the intramolecular vibrations that the internal normal modes have not only the same frequencies in the ground and excited state, but also that their minima were not displaced. This approximation restricts transitions between electronic states to vibrational transitions involving single quanta. The very slow rate of nonadiabatic transition inferred in the simulation is consistent with the hybrid model result that a more highly vibrationally excited ground state is the preferred product channel.

In the present paper, we address the roles of solvation dynamics and intramolecular dynamics on the ET rate by implementing a detailed molecular description of the solvated excited state in a calculation carried out in the spirit of the hybrid model. However, without the assumption about the character of the vibrational modes involved or of the solvation dynamics, this is done in terms of a Fermi golden rule rate expression in which the effect of solvation dynamics appears parametrically and the vibrational Franck−Condon contributions are calculated explicitly, although approximately. To do this, we extend the elements included in the previous mixed quantum classical simulations to explicitly include the full set of vibronic channels consistent with a detailed multidimensional displaced harmonic oscillator model of the solute.[20−22]

The paper is organized as follows. We present the theoretical and simulation methods implemented for this study in section 2. Section 3 reports and discusses the numerical results of the simulations followed by some concluding remarks in section 4.

II. Methods

Since the electronic transition of the ground to the first excited state of betaine-30 is the promotion of an electron from π orbital to a π^* antibonding orbital, the accurate treatment of electrons of the π subsystem is crucial to elucidate the intramolecular transition. Unlike conventional molecular dynamics (MD) simulations, therefore, we have to treat the key electronic degrees of freedom of π subsystem quantum mechanically and recalculate their wave functions at every MD time step. The electronic structure is calculated by employing the semiempirical Pariser−Parr−Pople (PPP) SCF method[23−25] with single excitation configuration interaction (CI). This method has proved quite adequate in reproducing the electronic transition energies of aromatic and conjugated systems.[26−30] The remaining electrons and nuclei are treated as effective classical nuclear cores. For core−core interactions, we include nonbonded interactions to correctly describe torsional motions by steric effects.[26] The excited-state energies are calculated from the diagonalization of the CI matrix. The most time-consuming part in the present simulations is the calculation of the excited-state forces, which are performed by the matrix inversion of the coupled perturbed Hartree−Fock equations.[31] For complete details, the reader is referred to earlier simulations.[14,15]

The CH_3CN molecules are realized as a rigid three site model with interaction sites at the atomic positions of the methyl carbon, carbon, and nitrogen. We use the solvent representation based on the OPLS force field[32] instead of that derived from ab initio calculations[33] since the former potential parameters are found to be superior in the ability to reproduce the observed spectral shifts.[12] One important difference between the two sets of parameters is that the dipole moment in the OPLS parameters is significantly smaller. The smaller dipole moment of solvent stabilizes the ground-state less and the energy gap between the ground and excited states becomes smaller.

A. Nonadiabatic Transition Rate. To calculate the nonadiabatic transition rate, we make use of the Kubo−Toyozawa approach[34] treating intramolecular high-frequency vibrations explicitly. In spirit of the Sumi−Marcus model,[2] we assume the transition rate can be taken as a function of solvation progress that is time-dependent. The rate can be calculated by averaging over many trajectories starting from different initial conditions rather than by evaluating the required free energy quantities.

In the lowest order of perturbation theory, the transition rate between two adiabatic states I and J is given by[35]

$$k_{J\rightarrow I} = \frac{1}{\hbar^2}\int \mathrm{d}\tau \exp\left\{\frac{i}{\hbar}\Delta E_{IJ}\tau\right\} \times \left\langle V_{IJ}(\tau) \exp_+\left\{-\frac{i}{\hbar}\int \mathrm{d}\tau' \Delta(\tau')\right\} V_{JI}(0)\right\rangle \quad (1)$$

where Δ and V_{IJ} are the diagonal and off-diagonal coupling terms, respectively. The energy gap is defined as $\Delta E_{IJ} \equiv E_J - E_I$ determined from the diagonalization of the CI matrix and $\exp_+$ denotes a positive time-ordered exponential operator. If we assume that the ground and excited states can be described by two identical mutually displaced multidimensional harmonic

surfaces, the diagonal coupling term is

$$\Delta = \sum_{\alpha} \omega_{\alpha}{}^{2}\delta_{\alpha}Q_{\alpha} + \frac{1}{2}\sum_{\alpha} \omega_{\alpha}{}^{2}\delta_{\alpha}{}^{2} \qquad (2)$$

where δ_α is the displacement of the equilibrium coordinate, ω_α is the frequency, and Q_α is the mass-weighted coordinate for α normal mode. In earlier studies,[21,22] the effects of the frequency shifts and Duschinsky rotations were not strong in the vibronic spectra of the simplest betaine pyridinium-*N*-phenoxide (R = H in Figure 1). The effects were also found to be small in the ET reaction between the tryptophan cation radical and tyrosine.[36] Therefore, we assume that the effects can be neglected in betaine-30, as well.

The adiabatic states depend parametrically on the nuclear coordinates and the off-diagonal coupling term is given by

$$V_{IJ} = \sum_{\alpha} \langle \Psi_I | P_\alpha | \Psi_J \rangle P_\alpha + \frac{1}{2}\langle \Psi_I | P_\alpha{}^{2} | \Psi_J \rangle \qquad (3)$$

where Ψ_I is the *I*th CI wave function and P_α is the corresponding momentum for α mode. Following the Kubo−Toyozawa approach,[34] we ignore the second term and assume $S_\alpha \equiv \langle \Psi_I | P_\alpha | \Psi_J \rangle$ to be independent of the nuclear coordinates. Then, the transition rate can be obtained as

$$k_{J\to I}(t) = \frac{1}{\hbar^2}\int \mathrm{d}\tau \exp\left\{\frac{i}{\hbar}\Delta E_{IJ}(t)\tau\right\} \times \exp\left\{\frac{1}{2\hbar}\sum_{\alpha}\delta_{\alpha}{}^{2}\omega_{\alpha}[\coth u_{\alpha}(\cos\omega_{\alpha}\tau - 1) - i\sin\omega_{\alpha}\tau]\right\} \times \left\{\left|\frac{1}{2\hbar}\sum_{\alpha}\delta_{\alpha}S_{\alpha}(t)\omega_{\alpha}[\coth u_{\alpha}(\cos\omega_{\alpha}\tau - 1) - i\sin\omega_{\alpha}\tau]\right|^{2} + \frac{1}{2\hbar}\sum_{\alpha}S_{\alpha}{}^{2}(t)\omega_{\alpha}[\coth u_{\alpha}\cos\omega_{\alpha}\tau - i\sin\omega_{\alpha}\tau]\right\} \qquad (4)$$

with $u_\alpha = \beta\hbar\omega_\alpha/2$. Note it is only the last term that allows the normal mode with zero displacement to contribute to the rate. The time-dependent rate $k_{J\to I}(t)$ is evaluated by taking an equilibrium average over initial vibrational states under the assumption that the vibrational relaxation is very fast. This assumption is in a similar spirit to that of the hybrid model.[4]

Since we neglect the frequency shifts and Duschinsky rotations, the values of ω_α can be obtained from the ground state. The geometry optimization and normal-mode analysis of the ground state for betaine-30 are performed with AM1 semiempirical Hamiltonian in the Gaussian 98 program.[37] To obtain the values of the displacement δ_α, the normal-mode analysis of the excited state should be performed but the number of atoms in betaine-30 makes the analysis intractable at a reliable level of the electronic Hamiltonian. Instead, we employ an approximate projection method. The normal coordinates of the ground state of betaine-30 are projected onto those of the simplest betaine obtained in previous works.[21,22] We make the reasonable assumption that the geometric structures and torsional degree of freedom of the central framework in the two betaines are similar to each other. The pendant rings in betaine-30 are not coplanar with this framework.[14,15] This assumption is also consistent with the fact that the effects of the frequency shifts and mode mixing are weak for the simplest betaine.[21,22] To find the most similar mode between the normal coordinates of betaine-30 and those of the simplest betaine, we calculate their inner products; the displacement δ_α of α mode of betaine-30 is taken as that of the simplest betaine that gives the maximum value of the inner product. If the maximum value of the inner products is smaller than a preselected value, we set $\delta_\alpha = 0$ assuming that no similar mode exists in the simplest betaine. (Betaine-30 has a large number of additional modes.) After calculating the intramolecular vibrational reorganization energy with the equation:

$\lambda_{B30}^{vib} = \Sigma_\alpha\, {}^1/_2\omega_\alpha\delta_\alpha{}^2$, we find that 0.3 as a preselected value produces a reasonable intramolecular vibrational reorganization energy, 4538 cm^{-1}.[4,13] Table 1 shows the frequencies of the 38 modes of betaine-30 with nonzero displacement that are determined by this process. For completeness, we note here that the solvent reorganization energy was determined previously[15] to be 3625 cm^{-1}.

TABLE 1: Sample Values of $|\langle S_\alpha \rangle|$ in a Dimensionless Unit[a]

$\lvert\langle S\rangle\rvert$	ω (cm^{-1})	$\lvert\langle S\rangle\rvert$	ω (cm^{-1})
0.403	1750.0	0.167	552.2
0.284	700.6	0.153	793.4
0.201	843.4	0.142	118.4
0.197	1212.5	0.135	1155.0
0.187	987.0	0.131	1337.2
0.186	1536.7	0.131	1695.1
0.185	728.7	0.129	1044.5
0.179	1613.4	0.126	1757.2
0.179	638.4	0.124	345.8
0.173	1669.4	0.121	1285.3

[a] The values are obtained by averaging the results of all time steps in 21 trajectories. The 20 largest values are listed.

We have also considered an alternative model where hydrogen atoms in the simplest betaine corresponding to the phenyl rings in betaine-30 have masses of C_6H_5. In order words, the model assumes that the betaine-30 has the same electronic structure as the simplest betaine except heavy-mass hydrogen atoms. In this case, projection is not required, and we can use the same values of δ_α as those in the simplest betaine, neglecting all other modes in betaine-30. We find no significant differences between results for electronic dynamics reported below that are determined for these two models, suggesting that the assumptions inherent in the projection approach are not crucial. Therefore, all the results below are calculated with the projection method. It should be noted that these methods are used only to find the values of δ_α and all the time-dependent simulations are done with the full betaine-30 molecule.

The energy gap ΔE and the nonadiabatic coupling matrix element S_α are time-dependent and should be recalculated at every time step. We neglect nonadiabatic coupling due to solvent motion, since it was found to be small in the previous simulation.[14,15] The value of S_α can be obtained from a calculation similar to that for the excited-state forces, but for the off-diagonal quantity $\langle \Psi_I | \partial/\partial R | \mathrm{Y}_J \rangle$. For the details and definitions of the required terms, the reader is referred to eqs 4 and 7 in ref.[14] We can make use of the linear transformation coefficients $\{l\}$ between the Cartesian and the normal mode coordinates as

$$\left\langle \Psi_I \middle| \frac{\partial}{\partial Q_{\mathrm{j}}} \Psi_J \right\rangle = \sum_i (l^{-1})_j{}^{i} \left\langle \Psi_I \middle| \frac{\partial}{\partial R} \Psi_J \right\rangle \qquad (5)$$

Denoting $S_J(t)$ as a survival probability that the system is still in the state J at t, the evolution equation

$$\frac{dS_J(t)}{dt} = -k_{J\to I}(t)S_J(t) \qquad (6)$$

can be integrated to obtain $S_J(t)$. Because the rate is dependent on the solvent coordinate that is time-dependent, the survival probability need not be exponential, in general.[34,35]

B. Simulation Methods. After an initial equilibration of a total of 1200 CH_3CN solvent molecules at 298.15 K, maintaining a solvent density of 0.78675 g/ cm^3, the betaine-30 molecule, in an equilibrium gas-phase structure, is inserted. Removing overlapping solvent molecules with the dye molecule makes the total number of solvent molecules 1172. The system is again equilibrated with the ground-state potential. The Nose−Hoover thermostat technique is used for equilibration.[38]

Initial ground state configurations to be photoexcited are prepared by running further equilibration for at least 5 ps with a time step of 2 fs to minimize correlations between trajectories. The photoexcitation is simulated by placing the betaine-30 molecule in the first excited state instantaneously. The ground state potential should then be replaced with that of the excited state from this vertical excitation time step. We assume that trajectories are adiabatic on the excited state and we do not calculate the surface hopping probability, unlike earlier simulations. The simulation of the excited state is basically the same as that of the ground state except that the Nose−Hoover technique is not used. To calculate the excited-state energies and forces efficiently, we consider only 50 single excitation configurations, which are chosen at every time step by selecting the 50 lowest energy diagonal elements of the CI matrix. For the transition to the first excited state, which is the only transition considered in the simulation, it is verified that the ground state absorption spectrum generated by these 50 configurations and all possible configurations are numerically comparable.

The neighbor list technique and periodic boundary condition are used and all the interactions are truncated with a smooth cutoff of half the box length. The equations of motion are integrated using the velocity Verlet algorithm with a time step of 2 fs. We use constraint dynamics such as RATTLE and SHAKE to keep the rigidity of the acetonitrile and the betaine-30 molecules.[39] The CH_3CN solvent molecules are realized as a rigid three site model. For betaine-30 molecule, we allow the six ring rotations and the single stretching motion of the central N−C bond, fixing all other degrees of freedom.

In the present work, we explicitly include the solute central N−C bond stretching motion, in addition to the ring torsional motions since the electronic distribution is expected to be coupled to this stretching motion. Electronic coupling across this bond connects the two charge centers in Figure 1. Hence, by including this motion explicitly, we allow the electronic distribution to be fully coupled to this degree of freedom. Nevertheless, there is a compromise here that needs to be noted. When treating the vibronic levels via normal modes in the rate expression, the contribution of this relatively low-frequency local motion to the energy gap is, in effect, included twice. As the number of normal modes active in the process will be seen to be rather large, we have accepted this inconsistency.

III. Results

To understand the details of the relaxation processes after photoexcitation, we plot the energy gap relaxation between the ground and the first excited states and central ring angle as a function of time in Figure 2. To minimize statistical noise, we have averaged 37 independent trajectories. First, we can observe the properties of the ground-state equilibrium from the data at $t = 0$. The averaged energy gap in the ground state is found to be 2.01 eV or 16200 cm^{-1}. This is a slightly smaller value than 17600 cm^{-1} in earlier simulations but very close to the experimental value of 16300 cm^{-1}.[40] This implies that the ground-state properties can be somewhat better described with the present set of parameters. The equilibrium central ring angle in the ground state is about 56°, which is a comparable value to the experimental value of 65° [41] or to other semiempirical calculation results of 48° [12] or 60°.[42]

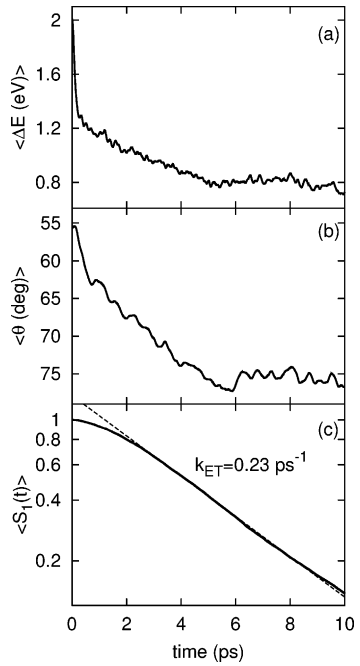

Figure 2. Time evolutions of (a) energy gap, (b) central ring angle, and (c) survival probability. The curve of survival probability is plotted on a semilog scale and the line of least-squares fit to the data for $t >$ 2 ps is indicated.

The photoexcitation involves the promotion of an electron from a π to a π^* orbital, resulting in an equilibrium central ring angle in the excited state of 90°, where the steric effects are also minimized. The most significant geometric change of betaine-30 due to the excitation should be that of the central ring angle θ, which can characterize the solute reorganization. The expected strong correlation between energy gap and θ is clearly seen in Figure 2, for times longer than 1 ps.

The dependences of the rate on the energy gap and the central ring angle are plotted in Figure 3. We average the accumulated results from all instantaneous ΔE and θ in 37 trajectories. One can notice the relatively larger statistical noise at small ΔE, since the energy gap is much less frequently small. The figure shows similar strong dependences of the rate on both ΔE and θ since they are correlated. The maximum rate in fact occurs at a relatively large energy gap, not at the smallest gap, mirroring the Franck−Condon density of vibronic states at that gap.[22] Similarly, the maximum rate occurs at around $\theta = 80°$ not at 90°. The fully twisted conformation is not an important one for the ET dynamics.

In Figure 2a, the energy gap is seen to drop rapidly over the first 0.2 ps of trajectories. This rapid drop of about 0.7 eV is dominated by the inertial motion of the solvent molecules subject to the different forces present on two electronic surfaces. Then, the energy gap reduces more slowly until about 5 ps. After 5 ps, no significant decrease of the energy gap is found. These different regimes can be also seen in the time dependence curve of central ring angle. The first one is the fast relaxation over the first 1 ps of trajectories followed by a slower relaxation phase until about 5 ps. And then the angle seems to diffuse

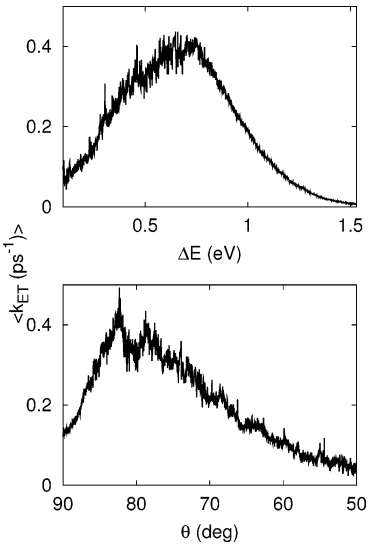

Figure 3. Averaged electron-transfer rate as a function of the energy gap (upper) and the central ring angle (lower).

around 75°, which can be understood by the fact that the potential surface regarding the rotation is relatively flat for large angle.[43]

Examining the two curves in parts a and b of Figure 2, we can characterize at least four relaxation time scales. The first one corresponds to the inertial solvent reorganization time scale for 0−0.2 ps. The second relaxation on the time scale of 0.21 ps is caused by the diffusive solvent reorganization. Then, the relaxation for 1−5 ps can be attributed to the solute reorganization represented by the change of the central ring angle. After 5 ps, both the solvent and the solute seem to be completely relaxed.

In Figure 2c, we plot the calculated survival probability as a function of time. The smooth curve obtained by averaging 37 trajectories shows that the relaxation rate is nearly constant after around 2 ps. The back transfer rate k_{ET} evaluated by a linear fit to the data for $t > 2$ ps is 0.23 ps^{-1} and the corresponding lifetime τ_{ET} is 4.35 ps. This value is much larger than 0.03 ps^{-1} of earlier simulations.[14] Since the major difference between the present and the earlier results is the improved inclusion of high-frequency internal molecular modes, this result numerically proves that the high-frequency vibronic channels play an important role in the ET reaction. However, the evaluated rate is smaller than the experimental results of 0.83[13] and 2 ps^{-1}.[4] Considering the character of the present model, particularly the approximate electronic structure for the excited state, we consider the agreement with experiment to be quite good, and sufficient to justify further analysis of the underlying components of the rate process.

Since the nonadiabatic coupling from each normal mode contributes to the ET reaction in a collective fashion, including potential cancellation in their sum, it is not straightforward to single out the magnitude of the contribution of each mode. Nevertheless, the value of $|\langle S_\alpha \rangle|$ may be used as a measure of the magnitude of the contribution, as seen in eq 4. The instantaneous values of $|\langle S_\alpha \rangle|$ in a representative set of 21 trajectories are averaged for each α mode and the 20 largest values are reported in Table 2. The largest contribution comes from the mode with $\omega = 1750.0$ cm^{-1}, which is very similar to the value ($\nu_{qm} = 1554$ cm^{-1}) of the single quantum mode used in earlier work.[4] However, Table 2 demonstrates clearly that it is not the single dominant contribution, and determination of the majority of the coupling requires a few dozen normal modes.

TABLE 2: Normal Mode Frequencies (cm^{-1}) and Displacements in the Ground State of Betaine-30[a] with Nonzero Displacement

mode	ω	δ	ω	ω	δ	mode	ω	δ
1	114.1	0.53	16	752.0	−0.41	31	1750.0	0.06
2	118.4	−5.96	17	793.4	−0.04	32	1757.2	0.06
3	125.3	0.20	18	901.2	0.41	33	1758.4	0.08
4	190.4	0.22	19	938.1	0.06	34	1763.3	−1.04
5	292.6	0.38	20	941.9	0.20	35	1779.5	0.02
6	320.8	−0.78	21	947.8	0.41	36	1807.6	0.02
7	433.5	−0.78	22	961.8	0.06	37	2007.6	0.31
8	445.3	0.22	23	963.3	0.03	38	3186.2	0.05
9	464.7	−0.57	24	971.4	0.20		.	.
10	552.2	0.03	25	1377.1	−0.16		.	.
11	578.8	−0.57	26	1379.8	−0.62		.	.
12	616.5	0.03	27	1570.0	−0.32		.	.
13	638.4	0.20	28	1593.1	0.30		.	.
14	678.0	0.07	29	1695.1	0.02		.	.
15	723.3	0.41	30	1726.0	−0.41		.	.

[a] AM1 Hamiltonian is used to perform a geometry optimization for the ground state.

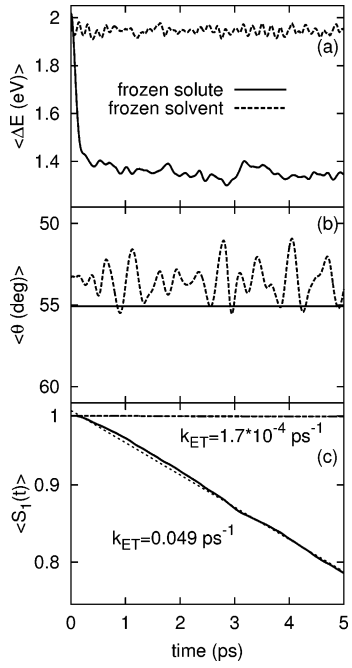

Figure 4. Time evolutions of (a) energy gap, (b) central ring angle, and (c) survival probability when the solute (solid line) or the solvent (dashed line) is frozen. The curve of survival probability is plotted on a semilog scale.

The rate obtained with only the three most important modes yields a rate only about 5% of the total, while using the largest six yields only 10%. This reinforces the importance of the use of multiple quantum modes rather than a single mode, in a realistic description.

To further analyze the observed multiple time scale relaxations, we carry out simulations for the cases that solute or solvent molecules are completely frozen. In Figure 4, the time profiles of energy gap, central ring angle, and survival probability are plotted for the frozen solute and solvent cases. We have averaged 20 trajectories for the frozen solute case, while only four trajectories are sufficient to see the impact for the frozen solvent case. In the frozen solute case, the initial rapid energy gap relaxation is nearly the same as in the normal case for the first relaxation period of 0−0.2 ps. The second relaxation regime of the diffusive solvent reorganization for 0.2−1 ps is observed but the solute reorganization regime disappears. Thus, the figure shows the dominance of the inertial solvent reorga-

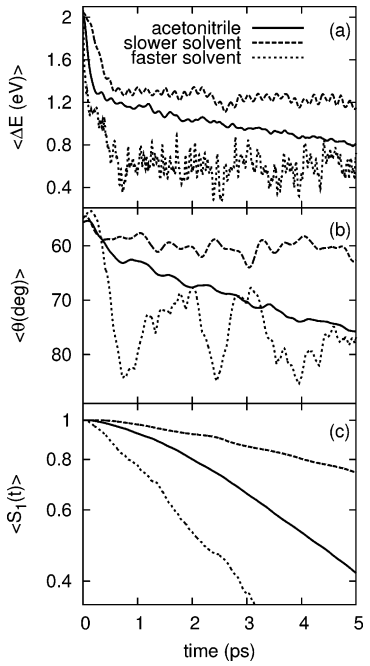

Figure 5. Time evolutions of (a) energy gap, (b) central ring angle, and (c) survival probability for slower and faster solvents than acetonitrile. The slower and faster solvents are realized by multiplying 10 and 0.1 to masses of atoms in acetonitrile, respectively. The curves for acetonitrile obtained by averaging the same four trajectories are added for comparison.

nization in the first period and the existence of the slower solvent reorganization period after that. In the frozen solvent case, no meaningful changes both for energy gap and central ring angle are observed since the frozen solvent environment prevents the solute reorganization too. The evaluated rates are far slower, 0.049 ps^{-1} and 1.0×10^{-4} ps^{-1} for the frozen solute and solvent cases, respectively. For the completely frozen solvent, a vastly slower rate is seen.

To check the ET rate dependence on the solvent relaxation rate, we have also considered a change in the masses of the solvent molecules. To mimic solvents which have slower and faster relaxation rates, we multiply all masses of the solvent atoms by 10 and by 0.1, respectively. We have averaged four trajectories for both cases. By the comparison with the relaxation curves in Figure 5, one can notice that the ring angle relaxation time is strongly affected by the solvent relaxation time. While, in the fast solvent case, the solute is fully relaxed on the order of 1 ps that is similar to the solvent relaxation time, the solute reorganization is very slow in the slow solvent case. As a result, the faster solvent gives the larger rate as noted earlier.[4] The evaluated rates for the faster and the slower solvents are 0.34 and 0.087 ps^{-1}, respectively.

IV. Conclusions

We have performed mixed quantum classical atomistic simulations of the intramolecular electron transfer reaction of betaine-30 in acetonitrile at room temperature. The π electronic degrees of freedom of the betaine-30 are treated quantum mechanically with the semiempirical PPP electronic structure method. The excited state dynamics is efficiently investigated with the single excitation configuration interaction method. The back electron transfer rate is evaluated by the time-dependent perturbation theory. The high-frequency internal vibrational modes are explicitly treated by assuming that the ground and excited states can be described by two identical mutually displaced multidimensional harmonic surfaces. The values of frequencies are obtained from the analysis of the ground state for betaine-30 and the values of displacements are obtained by using a projection method onto the modes of the simplest betaine. The evaluated back transfer rate k_{ET} is 0.23 ps^{-1}. This value is much larger than that in earlier simulations from our lab and comparable to the experimental results, with inclusion of a large number of the high-frequency vibronic channels.

The atomistic simulation results give a clear demonstration that multiple time scale relaxations are important to describe the election transfer dynamics correctly.[16−18] The fastest inertial time scale dominates the large initial subpicosecond relaxation. It is followed by the diffusive solvent relaxations on the picosecond time scale and then by a slow torsional angle relaxation of betaine-30. These multiple time scales are each indispensable for the proper description of the energy gap dynamics. We also find that the relaxation time scale of the torsional angle is strongly dependent on the mobility of the solvent molecules. Another important point of the present simulation results is that a relatively large number of high-frequency quantum modes participate in the electron transfer dynamics. While the hybrid model with a single quantum mode[4] captures correctly the idea that both the low and high frequency modes are important, multiple quantum modes are necessary to faithfully describe the electron transfer dynamics of the high dimensional molecular system. Further, the fact that solvation dynamics is found to be required to obtain a rate comparable to experiment suggests that even in solvents with relatively slow average relaxation times, observed ET rates likely reflect a significant component of ultrafast solvation dynamics.[16−18]

Thus, the present simulation results provide considerable new insight into the ultrafast intramolecular electron transfer reaction. By successfully capturing the effects of high-frequency and low-frequency quantum vibrational modes and contributions by solvation, the detailed molecular level results can be useful for the interpretation of experimental observations. The methods employed in this work to describe a delocalized electronic system should also be applicable to other interesting systems, including conductive polymers.[44]

Acknowledgment. The authors gratefully acknowledge the support of this research by a grant from the National Science Foundation (CHE0134775). Additional support was provided by the R. A. Welch Foundation (F-0019).

References and Notes

(1) Barbara, P. F.; Meyer, T. J.; Ratner, M. A. *J. Phys. Chem.* **1996**, *100*, 13148.
(2) Sumi, H.; Marcus, R. A. *J. Chem. Phys.* **1986**, *84*, 4894.
(3) Jortner, J.; Bixon, M. *J. Chem. Phys.* **1988**, *88*, 167.
(4) Walker, G. C.; Akesson, E.; Johnson, A. E.; Levinger, N. E.; Barbara, P. F. *J. Phys. Chem.* **1992**, *96*, 3728.
(5) Reichardt, C. *Chem. Rev.* **1994**, *94*, 2319.
(6) Reid, P. J.; Barbara, P. F. *J. Phys. Chem.* **1995**, *99*, 3554.
(7) Zong, Y. P.; McHale, J. L. *J. Chem. Phys.* **1997**, *106*, 4963.
(8) Zong, Y. P.; McHale, J. L. *J. Chem. Phys.* **1997**, *107*, 2920.
(9) Hogiu, S.; Werncke, W.; Pfeiffer, M.; Elsaesser, T. *Chem. Phys. Lett.* **1999**, *312*, 407.
(10) Hogiu, S.; Dreyer, J.; Pfeiffer, M.; Brzezinka, K. W.; Werncke, W. *J. Raman Spectrosc.* **2000**, *31*, 797.
(11) Hogiu, S.; Werncke, W.; Pfeiffer, M.; Dreyer, J.; Elsaesser, T. *J. Chem. Phys.* **2000**, *113*, 1587.
(12) Mente, S. R.; Maroncelli, M. *J. Phys. Chem. B* **1999**, *103*, 7704.
(13) Kovalenko, S. A.; Eilers-Konig, N.; Senyushkina, T. A.; Ernsting, N. P. *J. Phys. Chem. A* **2001**, *105*, 4834.
(14) Lobaugh, J.; Rossky, P. J. *J. Phys. Chem. A* **1999**, *103*, 9432.
(15) Lobaugh, J.; Rossky, P. J. *J. Phys. Chem. A* **2000**, *104*, 899.
(16) Zhu, J. J.; Rasaiah, J. C. *J. Chem. Phys.* **1994**, *101*, 9966.
(17) Gayathri, N.; Bagchi, B. *J. Chim. Phys.* **1996**, *93*, 1652.

(18) Bagchi, B.; Gayathri, N. *Adv. Chem. Phys.* **1999**, *107*, 1.
(19) Maroncelli, M. *J. Mol. Liq.* **1993**, *57*, 1.
(20) Hwang, H.; Rossky, P. J. *J. Chem. Phys.* **2004**, *120*, 11380.
(21) Hwang, H.; Rossky, P. J. *J. Phys. Chem. B* **2004**, *108*, 6723.
(22) Hwang, H.; Rossky, P. J. *J. Phys. Chem. A* **2004**, *108*, 2607.
(23) Pariser, R.; Parr, R. G. *J. Chem. Phys.* **1953**, *21*, 466.
(24) Pariser, R.; Parr, R. G. *J. Chem. Phys.* **1953**, *21*, 767.
(25) Pople, J. A. *Trans. Faraday. Soc.* **1953**, *49*, 1375.
(26) Murrell, J. N.; Harget, A. J. *Semiempirical Self-Consistent Molecular-Orbital Theory of Molecules*; Wiley-Interscience: London, 1972.
(27) Warshel, A.; Karplus, M. *J. Am. Chem. Soc.* **1972**, *94*, 5612.
(28) Karabunarliev, S.; Baumgarten, M.; Mullen, K. *J. Phys. Chem. A* **2000**, *104*, 8236.
(29) Wong, K. F.; Skaf, M. S.; Yang, C. Y.; Rossky, P. J.; Bagchi, B.; Hu, D. H.; Yu, J.; Barbara, P. F. *J. Phys. Chem. B* **2001**, *105*, 6103.
(30) Wong, K. F.; Bagchi, B.; Rossky, P. J. *J. Phys. Chem. A* **2004**, *108*, 5752.
(31) Pople, J. A.; Krishnan, R.; Schlegel, H. B.; Binkley, J. S. *Int. J. Quantum Chem.: Quantum Chem. Symp.* **1979**, *13*, 225.
(32) Jorgensen, W. L.; Briggs, J. M. *Mol. Phys.* **1988**, *63*, 547.
(33) Edwards, D. M. F.; Madden, P. A.; Mcdonald, I. R. *Mol. Phys.* **1984**, *51*, 1141.
(34) Kubo, R.; Toyozawa, Y. *Prog. Theor. Phys.* **1955**, *13*, 160.
(35) Egorov, S. A.; Rabani, E.; Berne, B. J. *J. Chem. Phys.* **1999**, *110*, 5238.
(36) Lee, E.; Medvedev, E. S.; Stuchebrukhov, A. A. *J. Chem. Phys.* **2000**, *112*, 9015.
(37) Frisch, M. J.; Trucks, G. W.; Schlegel, H. B.; Scuseria, G. E.; Robb, M. A.; Cheeseman, J. R.; Zakrzewski, V. G.; Montgomery, J. A., Jr..; Stratmann, R. E.; Burant, J. C.; Dapprich, S.; Millam, J. M.; Daniels, A. D.; Kudin, K. N.; Strain, M. C.; Farkas, O.; Tomasi, J.; Barone, V.; Cossi, M.; Cammi, R.; Mennucci, B.; Pomelli, C.; Adamo, C.; Clifford, S.; Ochterski, J.; Petersson, G. A.; Ayala, P. Y.; Cui, Q.; Morokuma, K.; Malick, D. K.; Rabuck, A. D.; Raghavachari, K.; Foresman, J. B.; Cioslowski, J.; Ortiz, J. V.; Baboul, A. G.; Stefanov, B. B.; Liu, G.; Liashenko, A.; Piskorz, P.; Komaromi, I.; Gomperts, R.; Martin, R. L.; Fox, D. J.; Keith, T.; Al-Laham, M. A.; Peng, C. Y.; Nanayakkara, A.; Gonzalez, C.; Challacombe, M.; Gill, P. M. W.; Johnson, B.; Chen, W.; Wong, M. W.; Andres, J. L.; Gonzalez, C.; Head-Gordon, M.; Replogle, E. S.; Pople, J. A. *Gaussian 98, Revision A.7*; Gaussian, Inc.: Pittsburgh, PA, 1998.
(38) Frenkel, D.; Smit, B. *Understanding Molecular Simulation: from algorithms to applications;* Academic Press: San Diego, CA, 1996.
(39) Allen, M. P.; Tildesley, D. J. *Computer Simulation of Liquids;* Oxford University Press: Oxford, U.K., 1987.
(40) Reichardt, C. *Angew. Chem., Int. Ed. Engl.* **1979**, *18*, 98.
(41) Allmann, R. *Z. Kristallogr.* **1969**, *128*, 115.
(42) Bartkowiak, W.; Lipinski, J. *J. Phys. Chem. A* **1998**, *102*, 5236.
(43) Ishida, T.; Rossky, P. J. *J. Phys. Chem. A* **2001**, *105*, 558.
(44) Aldissi, M. *Intrinsically conducting polymers: an emerging technology;* Kluwer Academic: Dordrecht, The Netherlands, 1993.